Nano and Micro-hydroxyapatite Particles for Lead Removal from Wastewater

CLAUDIA MARIA SIMONESCU[1], ALINA TATARUS[1], CHRISTU TARDEI[2]*, DELIA PATROI[2], MIOARA DRAGNE[3], DANIELA C. CULITA[4], RODICA-ELENA PATESCU[1], LAURENTIU TEODOR BUSUIOC[1], IOANA MELINTE[1]

[1] University Politehnica of Bucharest, Faculty of Applied Chemistry and Materials Science, 1-7 Polizu Str., 011061 Bucharest, Romania

[2] National Institute for R&D in Electrical Engineering ICPE-CA, 313 Splaiul Unirii, 030138, Bucharest, Romania

[3] SC KEMCRISTAL SRL, 51 Muncii Str., Fundulea, Călăraşi, Romania

[4] Romanian Academy, Institute of Physical-Chemistry "Ilie Murgulescu", 202 Splaiul Independentei, 060023, Bucharest, Romania

Two types of ($Ca_{10}(PO_4)_6(OH)_2$) hydroxyapatite (HAP) powders with high purity were obtained using two different synthesis methods – a wet chemical synthesis method such as precipitation from aqueous solution and a dry chemical method such as solid-state sintering. Both types of powders were characterized by X-ray diffraction, FT-IR analysis, scanning electron microscopy (SEM), and N_2 sorption analysis. X-ray diffraction showed that both HAP powders contain hydroxyapatite as the only crystalline phase. Data from X-ray diffraction were confirmed by FT-IR spectra. SEM images showed that nanometric size hydroxyapatite (nano-HAP) was obtained by precipitation from aqueous solution and hydroxyapatite with micrometric size (micro-HAP) was obtained using sintering method as a solid phase synthesis method. Nano-HAP powder has a BET surface area almost 5 times higher than that of the microcrystalline HAP powder. Consequently, both powders were comparatively tested in lead removal process from aqueous solutions. The contact time, the concentration of lead ions in the initial solution, pH and temperature were the main parameters studied. The highest Pb(II) sorption was achieved for nano-HAP. The sorption process was relatively fast because the equilibrium was achieved after about 60-180 min of contact depending on the lead concentration in the initial solution, and the specific surface area of the samples. Results showed that the adsorption behaviour of micro-HAP and nano-HAP follows the Langmuir isotherm. The kinetic process of Pb(II) sorption onto micro-HAP and nano-HAP was tested by applying the pseudo-first order, the pseudo-second order, and intraparticle diffusion models. The experimental data were fitted with pseudo-second order equation. The main mechanism for lead ions removal using synthesized micro-HAP and nano-HAP was suggested to be dissolution of HAP followed by hydroxy-pyromorphite ($Pb_5(PO_4)_3OH$) precipitation. From this experimental study, it can be concluded that both sorbents can be successfully applied for lead removal from wastewater.

Keywords: sintering, calcination, porosity, hydroxiapatite, environmental applications

Environments contaminated with metals have been extensively studied in recent years, due to the negative effects of the heavy metals on living organisms (plants, animals, humans) [1]. Their negative effects are due to their toxicity, persistence, bioaccumulation and bio-magnification through chain food [2]. Therefore, considerable effort has been made to treat and remediate environments contaminated with heavy metals.

Chemical precipitation, ionic exchange, flotation, reverse osmosis, sorption, membrane filtration and electrochemical methods are used as traditional methods to remediate wastewater with heavy metals content [3]. From these techniques, sorption has flexibility in design and operating conditions, leading to effluents with very low content of heavy metals [4]. Another advantage of the sorption process is the fact that sorbents can be regenerated by desorption and they can be reused in several sorption cycles [5]. The sorption process is characterized by low cost, as compared with other heavy metals removal traditional methods. This process is considered one of the most important processes of removing heavy metals from various wastewater sources [6].

Numerous materials such as clays [7], unmodified and modified starch [8], activated carbon, bone meal and iron fines [9], metal oxides and hydroxides [10, 11], by products [12], cellulose [13], carbon nanotubes [14], natural and synthetic zeolites [15], composite materials [16], polymers and hydrogels [17, 18], phosphates [19], saline slags [20], fly ash [21], biomass-derived sorbents [22] have been employed as adsorbents for removal of heavy metals from wastewater and aqueous solutions.

It has been demonstrated that the following three steps are involved in heavy metals removal by sorption onto solid sorbents (1) the transport of the heavy metal from the bulk solution to the sorbent surface; (2) adsorption on the particle surface; and (3) transport within the sorbent particle [4]. Selection of the most suitable sorbent to treat wastewater with heavy metals content has to be made taking account by the technical applicability and cost-effectiveness. Thus, intense efforts have been aimed at the development of new heavy metals adsorbents with good sorption capacity, selectivity and low cost [23].

Hydroxyapatite is an important biomaterial studied for applications in medicine [24]. Due to its chemical structure, and structural similarity with the mineral component of bones and teeth, HAP is often used for hard tissue repair. HAP may be used in the form of powder or as composite particles coated with various organic compounds [25]. The use of calcium phosphate as adsorbent is due to its large specific area, high thermal and chemical stability, and high ionic exchange capacity.

* *email: christu.tardei@icpe-ca.ro*

As it is known, the crystal structure of hydroxyapatite, $(A_4^{I})(A_6^{II})(BO_4)_6(X_2)$, allows a high degree of structural disorder due to multiple chemical substitutions. Metal cations can replace Ca^{2+} ions while anions with similar structure can substitute PO_4^{3-} groups. Keeping the neutrality of the compound allows substitutions in either position [26]. Basically, these substitutions distort the crystalline network, inherent defects contributing to increased network adsorption capacity, easily retaining impurities on ceramic compound. All these properties along with other important properties such as low water solubility, high specific surface area suggest that HAP can be an effective sorbent for heavy metals environments remediation. Natural or synthetic HAP has been used for treatment processes. Laboratory synthesis of HAP is performed also to modify its physical and chemical properties, but also to preserve natural mineral reserves, this being one of the most important sustainable development principles. Physical and chemical properties of hydroxyapatite, closely related to chemical reactivity, are strongly influenced by the preparation method and experimental conditions. Many researchers have tried to modify the HAP properties such as biological activity, mechanical strength, solubility and sinterability by controlling the composition, morphology, and particle size, through different synthesis methods, and/or modifying the synthesis conditions in order to use it in different applications [27, 28]. Several forms of particulate products are used as solid sorbents for removal of heavy metals from wastewater, including irregular multifaceted particles and rounded smooth granules with solid or porous structures [29].

For the synthesis of nano- and micrometric HAP particles, several methods such as chemical precipitation [30], hydrothermal synthesis [31], sol-gel methods [32], multiple cross-linked emulsion techniques [33], biomimetic deposition techniques [34], electrodeposition [35], synthesis in the ultrasonic field [36] have been used.

To obtain materials with well-defined and reproducible properties, rigorous testing and regulating the working parameters in all stages of synthesis are required. Thus, this experimental study was performed in order to develop two types of HAP powders, one of them of nanometric size using unconventional techniques such as precipitation from aqueous solutions, and the other one of micrometric size by the solid phase sintering reaction. Both types of powders were structurally and morphologically characterized. An important objective of this research study was to investigate the possible use of HAP particles in the removal of soluble lead(II) ions from synthetic solutions. By achieving this goal, new information on the synthesis, sintering, characterization, and using of micro- and nanosized HAP for the remediation of heavy metals contaminated environments will be provided.

Experimental part

Materials and methods

Raw materials such as $(NH_4)_2HPO_4$, $Ca(NO_3)_2{\cdot}4H_2O$, $Pb(NO_3)_2$ used for the experiments were obtained from Merck, all of analytical grade. $CaHPO_4{\cdot}2H_2O$ and $CaCO_3$ were also of analytical grade, and they were obtained from Fluka. 25% NH_3 solution (NH_4OH), 63% HNO_3 and 0.1M HNO_3 solutions analytical grade, Fluka origin were used for *p*H adjustment using.1000 mg/L stock lead(II) solution was prepared by dissolving 1.5986 g of $Pb(NO_3)_2$ in 1L distilled water. The required concentration of Pb(II) solution was obtained by serial dilution of 1000mg/L Pb(II) solution.

Hydroxyapatite preparation

Hydroxyapatite preparation by chemical precipitation

A wet synthesis method was used to obtain HAP particles. This involves *p*H higher than 8 (to ensure the apatite structure formation) and reaction temperature between 25 and 90°C. Higher temperatures favour the formation of compounds with high degree of crystallinity. Precipitation method used involves precursors such as $Ca(NO_3)_2{\cdot}4H_2O$ and $(NH_4)_2HPO_4$ at a stoichiometry corresponding to $Ca_{10}(PO_4)_6(OH)_2$ for which the ratio Ca/P is 1.67. Preparation of hydroxyapatite was carried out under specified conditions of temperature and *p*H, according to the overall reaction presented below:

$$10[Ca(NO_3)_2{\cdot}4H_2O]+6(NH_4)H_2PO_4+ \\ +\ 8\ NH_4OH=Ca_{10}(PO_4)_6(OH)_2+20NH_4NO_3+6H_2O \qquad (A)$$

The solutions of $Ca(NO_3)_2$ and $(NH_4)H_2PO_4$ were separately prepared and stirred for 30 min . Then, $(NH_4)_2HPO_4$ solution was slowly added to the $Ca(NO_3)_2{\cdot}4H_2O$ solution and pH was increased to 9 using NH_4OH. The reaction mixture was heated to 40-60 °C for 120 min and stirred intensively. During the reaction, the pH was controlled in order to keep it above 8. Then the suspension was kept under the mother liquid conditions for 15 h at room temperature for aging. The precipitate was filtered through Whatman 41 filter paper, washed three times with doubly distilled water, dried at 110 °C for 12 h to eliminate retained water and calcined at 900-1200°C for 2 h.

Hydroxyapatite preparation by solid-state sintering

For the synthesis of hydroxyapatite by conventional solid-state ceramic method, high purity calcium carbonate and phosphate salts are generally used as raw materials. Stoichiometric mixtures of starting materials were homogenized by ball milling (Fritsch-type Planetary Mill Pulverisette 5) for 6 h in an aqueous medium in order to get hydroxyapatite compound. The dry material (moisture content <5%) was calcined at 1200°C. The formation of the compound was achieved by a sequence of reactions at temperatures between 210 and 1200°C. The general process for HAP particles obtaining is shown in the following reaction:

$$4CaCO_3(s) + 6CaHPO_4{\cdot}2H_2O\ (s) \rightarrow \\ Ca_{10}(PO_4)_6(OH)_2\ + 4CO_2(g) + 14H_2O(g) \qquad (B)$$

Testing techniques

All hydroxyapatite ceramic powders were characterized using FT-IR spectroscopy, X-ray diffraction (XRD), scanning electron microscopy (SEM) and BET surface area and porosity measurements.

The crystal phase was identified by powder X-ray diffraction (XRD) using X-ray diffractometer D8 ADVANCE-GERMANY type with Cu Kα radiation (k = 1.5404 A°) and XPERT software.

The presence of functional groups was analyzed by FT-IR spectroscopy using a SHIMADZU FTIR 8400 Spectrometer in the 400-4000 cm^{-1} range.

Scanning electron microscopy (SEM) analysis was performed using a Carls Zeiss Auriga scanning electron microscope. For the analysis by this technique, samples were subject to a special process of preparation by cleaning for 6 min in plasma arc in a Plasma Cleaner FISCHONE Device.

Nitrogen sorption isotherms at -196°C were recorded on a Micromeritics ASAP 2020 automated gas adsorption

system. Samples were degassed at 200°C for 4 h under vacuum prior to the N_2 adsorption. Specific surface areas (S_{BET}) were calculated according to the Brunauer-Emmett-Teller (BET) equation using adsorption data in the range of 0.05 to 0.30 relative pressures. Total pore volume (V_{total}) was estimated from the total volume of nitrogen adsorbed at the relative pressure of 0.99. The pore size distribution curves were obtained using the Barrett-Joyner-Halenda (BJH) model from the desorption branch.

Sorption experiments

Metal ion concentration in the initial solutions and in solutions after the sorption on nano and micro-HAP were determined by atomic absorption spectrometry using an AAS 1N Carl Zeiss Jena Atomic Adsorption Spectrophotometer.

For studying the sorption capacity of micro- and nano-HAP for the removal of Pb(II) from aqueous solutions, batch adsorption experiments were performed varying different parameters. Experiments were performed at room temperature (21 ± 2°C) by diluting the stock solutions of Pb(II). Dilution was done to obtain solutions in the range of 5–100 mg/L.

Batches of metal solution and adsorbent were run for the contact time (0–360 min). Various parameters such as *p*H(2–6), sorbent dose (0.05–0.5g), initial metal concentrations (5–100 mg/L) and temperature (20–40°C) were studied in the given respective ranges, to obtain the optimum conditions for adsorption to occur. The contact between these two phases (solid - HAP and liquid - lead synthetic solutions) was performed using a GFL Shaker 3015 at 150 rpm.

The amount of lead ions adsorbed by micro- and nano-HAP particles (mg/g), and the removal efficiency (%) were calculated using eqs. (1) and (2).

$$Q = \frac{(C_i - C_f)\cdot V}{m} \quad (1)$$

where:

Q – lead uptake (mg/g);

C_i - the concentration of lead ions in the initial solution (mg/L);

C_f - the concentration of lead ions remaining in solution at various times (mg/L);

V - volume of the solution (L) and m - mass of micro- and nano-HAP used (g).

$$\eta = \frac{(C_i - C_f)}{C_i}\cdot 100 \quad (2)$$

where:

η is removal efficiency (%);

C_i - the concentration of lead ions in the initial solution (mg/L);

C_f - the concentration of lead ions remaining in solution at various times (mg/L).

For each sorption experiment, the average of three replicates was reported.

Results and discussions

Hydroxyapatite preparation and characterization

HAP particles obtained were characterized using FT-IR spectroscopy, X-ray diffraction, scanning electron microscopy and BET surface area determination.

The FT-IR spectra of the HAP samples obtained by chemical precipitation and solid-state sintering are shown in figure 1 and 2.

Both spectra agreed well with the reported IR data for HAP materials. Thus, the peaks at approximately 464, 568, 603, 963, 1064 and 1089 cm^{-1} were characteristic bands for PO_4^{3-}, and the peaks at 3572 and 1640 cm^{-1} were the bending mode of the absorbed water [36]. Absence of any distinct bands in the range of 1400-1500 cm^{-1} indicates that HAP does not contain carbonate ions.

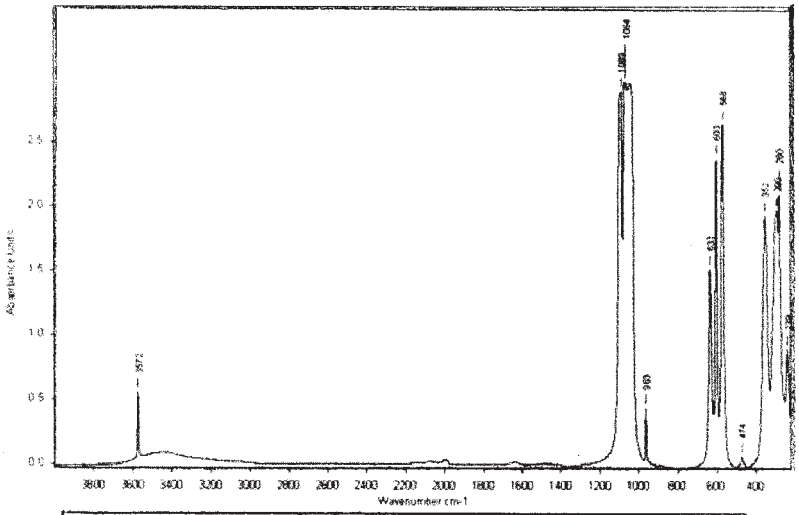

Fig. 1. FT-IR spectra of HAP particles obtained by chemical precipitation

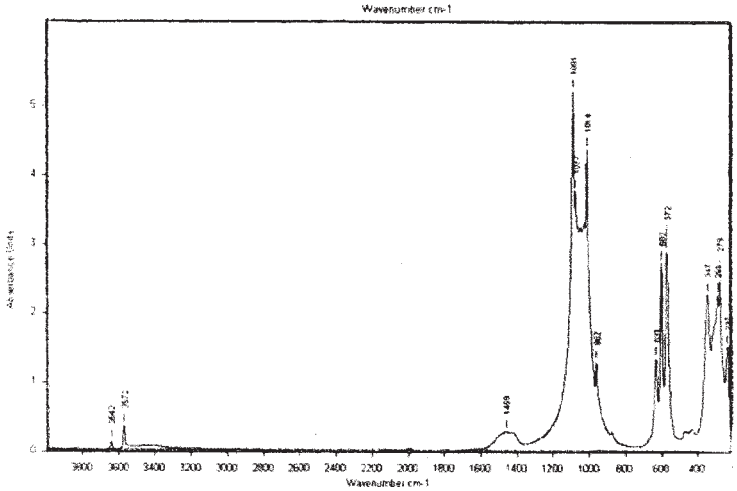

Fig. 2. FT-IR spectra of HAP particles obtained by solid-phase sintering

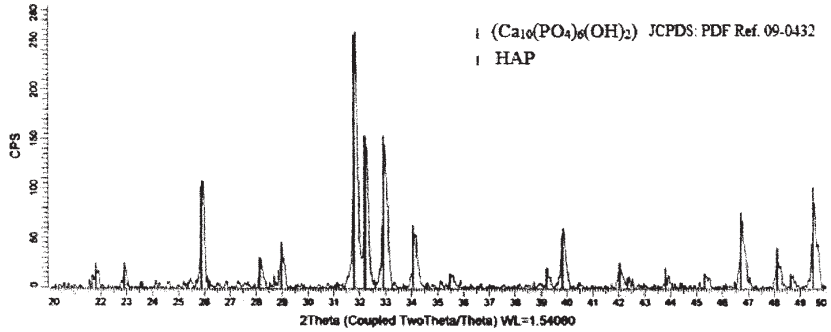

Fig. 3. XRD pattern of HAP particles obtained by chemical precipitation

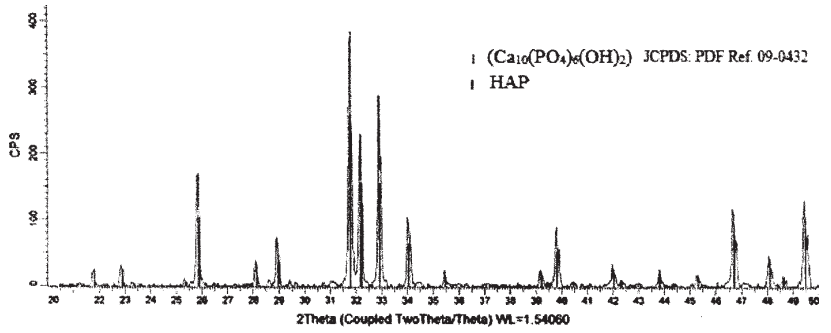

Fig. 4. XRD pattern of HAP particles obtained by solid-phase sinterin

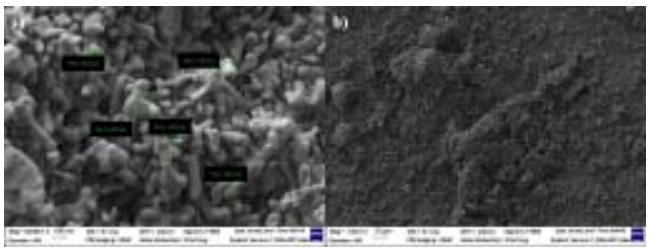

Fig. 5. SEM micrographs of hydroxyapatite obtained by chemical precipitation (a) magnification – 100,000X, 2.00 kV, and (b) magnification 1,000X, 2.00 kV)

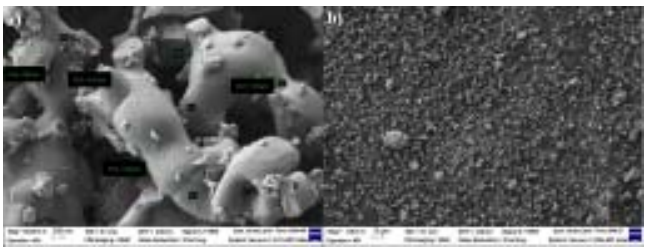

Fig. 6. SEM micrographs of hydroxyapatite obtained by solid-phase sintering (a) magnification – 50,000X, 2.00 kV, and (b) magnification – 1,000X, 2.00 kV)

In case of HAP particles obtained by sintering method, the IR spectrum (fig. 2) showed presence of peaks at approximately 571, 602, 962, 1014, 1077 and 1091 cm^{-1} characteristic for PO_4^{3-}, and peak at 3572 cm^{-1} characteristic for water molecules [36]. The small peak at 1459 cm^{-1} was attributed to carbonate ions.

Figures 3 and 4 show the XRD patterns of the HAP particles obtained by chemical precipitation and solid-phase sintering method.

As noted, both samples exhibit the characteristics of HAP reported in the literature [36]. HAP characteristic bands assignment was made according to JCPDS standard No. 09-0432. No impurity peak was observed in the XRD patterns of both HAP samples indicating that the hydroxyapatite was the only crystalline phase.

Scanning electron microscopy (SEM) was used for microstructural characterization of HAP samples. The SEM micrographs of the HAP sample obtained by chemical precipitation are presented in figures 5a, b.

As can be seen the sample consist of little ovoidal particles with average dimensions less than 100 nm and some aggregates of ~ 300-400 nm. The sample also contains particles of spherical shape with average diameters of 80 nm. The microstructure consists of small pores (average diameters of 100-200 nm) which always exist on grain boundaries and enclosed by several grains in the proximity, as presented in the figure 5b.

The SEM images of samples calcined at 1200°C (fig. 6a, b) showed that hydroxyapatite micrometric powder obtained by solid-state sintering method have high amount of pores with average diameter of ~1μm, in contrast with nano-hydroxyapatite powder which showed a dense microstructure.

The particles exhibit an irregular hexagonal morphology. As illustrated in figures 6a, b, it is clearly observed that the grains become bigger as the calcination temperature increases. The particles attached to each other to form larger and more compact aggregates due to the heat treatment, as shows in figure 6a. The microstructures of the two hydroxyapatite powders showed remarkable differences in their sizes and shapes.

The results of BET surface area and porosity measurements show that HAP powder obtained by precipitation method has a BET surface area of 11.3 m^2/g, a total pore volume of 0.041 cm^3/g and an average pore diameter of 17.3 nm. The HAP powder obtained by solid state sintering method has a BET surface area of 2.3 m^2/g, a total pore volume of 0.009 cm^3/g and the average pore diameter of 21.3 nm.

These data let us suppose that nano-HAP powder synthesized by chemical precipitation method could have a higher sorption capacity than micrometer HAP powder obtained by solid state sintering method (having a BET surface area ~5 times higher than that of the micro-crystalline powder). Consequently, the powders obtained were tested for the sorption process of lead from aqueous solutions.

Sorption experiments

Effect of contact time

Lead adsorption studies were carried out as a function of contact time. The adsorption capability of HAP microbeads was compared with that of HAP nanoparticles in figures 7, 8.

From figures 7 and 8 it can be seen that the retention of lead ions from synthetic solutions by nano and

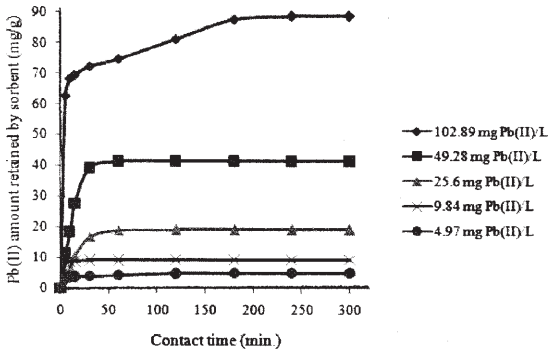

Fig. 7. Influence of contact time on the Pb(II) amount retained by micro-HAP at different lead concentrations in the initial solution

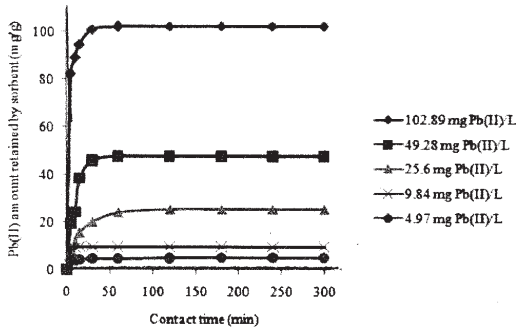

Fig.8. Influence of contact time on the Pb(II) amount retained by nano-HAP at different lead concentrations in the initial solution

microparticles of HAP is a rapid process because equilibrium was reached after approximately one or three hours depending on the lead concentration in the initial solution. Increasing contact time between the two phases determines increasing of the amount of lead ions retained on nano-HAP and micro-HAP particles. The short time necessary to reach the equilibrium indicates strong interactions between Pb(II) and HAP nano and micro-particles. HAP nanoparticles have a higher sorption capacity compared to HAP microparticles. The maximum amount of Pb(II) retained per gram of nano-HAP is 102.45 mg/g, while the maximum amount of Pb(II) retained per gram of micro-HAP is 88.46 mg/g. These values are comparable with the literature data [37].

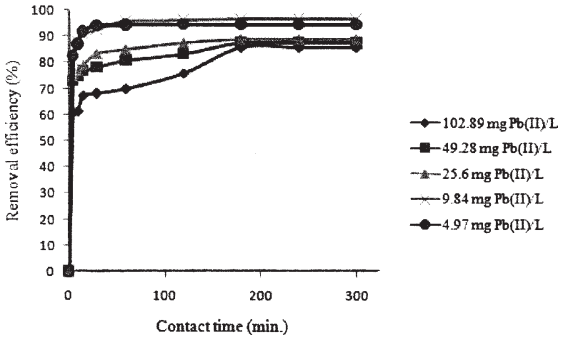

Fig. 9. Influence of contact time on the Pb(II) removal efficiency by micro-HAP at different lead concentrations in the initial solution

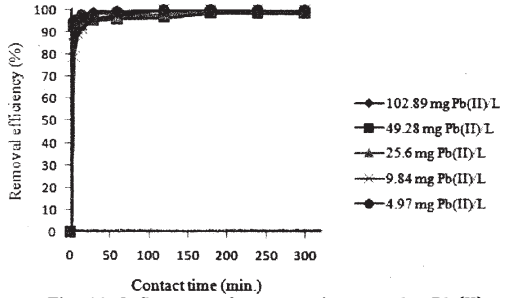

Fig. 10. Influence of contact time on the Pb(II) removal efficiency by nano-HAP at different lead concentrations in the initial solution

The plot of variation of removal efficiency of Pb(II) against contact time (eq. 2) is presented in figures 9, 10.

It can be seen that the removal efficiency increases with the increasing of the contact time between the two phases. The maximum value of removal efficiency of micro-HAP is 96.56%, while in case of nano-HAP is 99.99%. These results reveals that the nano-HAP has a higher removal efficiency than micro-HAP.

The high speed of the removal process and the high value of the removal efficiency may lead to the conclusion that the synthesized nano and micro-HAP particles can be successfully used in the retention of lead ions from synthetic solutions and wastewater.

Effect of pH on lead removal process

*p*H is considered one of the parameters that significantly influences the metal ions adsorption process. In our case, this is due to the fact that HAP particles exhibit *p*H-dependent surface charge, and the percent of various heavy metal hydrolytic species depend on *p*H [68]. The initial *p*H of solutions varied from 2.0 to 6.0. Higher values of *p*H have not been chosen for experiments because, according to the hydrolysis constant of Pb(II) ($logk_1$ = 6.48, $logk_2$ = 11.16, and $logk_3$ = 14.16) [69, 70], the lead hydroxyl components are the dominant species in the range of 7-12. Thus, these species can hinder the direct interaction between lead ions and the active sites of HAP [37].

The relation between the initial *p*H of the solution and the amount of Pb(II) retained by the micro and nano-HAP particles is shown in the figures 11 and 12.

From these figures it can be observed that in the lower initial *p*H range the amount of lead adsorbed by micro- and nano-HAP particles increases with the increasing of *p*H value till it reaches a maximum value. This increasing is not significant, 8.6 mg/g for micro-HAP and 2.4 mg/g for nano-HAP. The low values of adsorption at very low *p*H values could be the result of the competition between protons and lead ions at the sorption sites, with a preponderance of protons which hinder the approach of lead ions as a result of repulsive forces. After reaching the maximum sorption capacity at *p*H 3.5, a decrease of the adsorbed Pb(II) amount with the increase of *p*H was observed. This could be due to both loading of all HAP

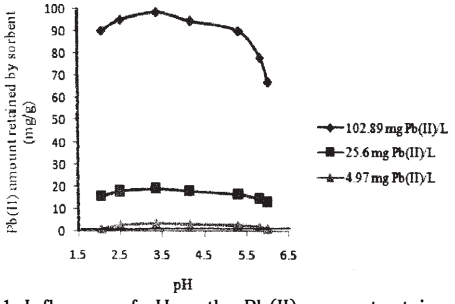

Fig. 11. Influence of *p*H on the Pb(II) amount retained by micro-HAP at different concentrations of the initial solution

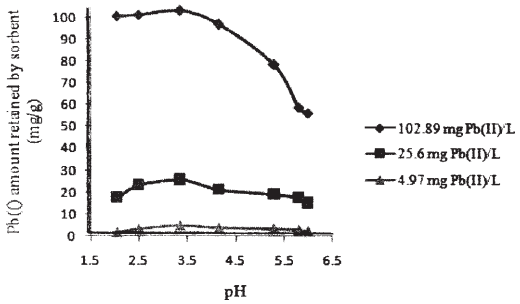

Fig. 12. Influence of pH on the Pb(II) amount retained by nano-HAP at different concentrations of the initial solution.

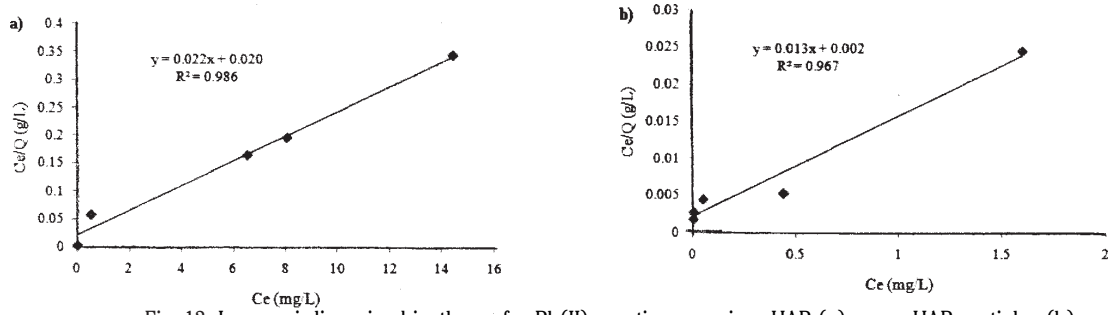

Fig. 13. Langmuir linearized isotherm for Pb(II) sorption on micro-HAP (a); nano-HAP particles (b)

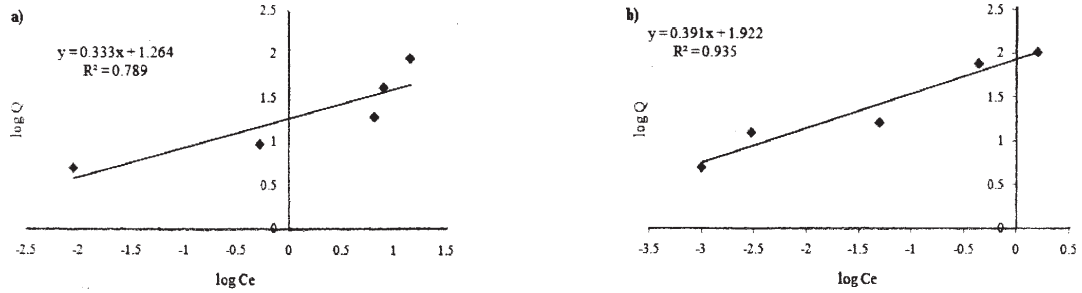

Fig. 14. Freundlich linearized isotherm for Pb(II) sorption on micro-HAP (a) and nano-HAP particles (b)

Sorbent	Langmuir isotherm			Freundlich isotherm		
	Q	a	R^2	K_F	n	R^2
micro-HAP	88.46	1.1	0.986	2.155	1.264	0.789
nano-HAP	102.45	6.5	0.967	2.183	1.922	0.935

Table 1
LANGMUIR AND FREUNDLICH CONSTANTS AND CORRELATION COEFFICIENTS FOR ADSORPTION OF PB(II) ON MICRO- AND NANO-HAP

sorption sites with lead ions and precipitation of insoluble lead hydroxide. Also, it can be observed that at low Pb(II) concentrations in the initial solution, the total amount of Pb(II) removed from the solution was pH-independent in both types of adsorbents (micro- and nano-HAP). This finding is consistent with literature data [38].

Adsorption isotherms and kinetics

It is well known that, the relationship between the metal ions concentration in the solution and the amount of metal ions adsorbed on the solid phase at the equilibrium is expressed by sorption isotherm. Batch approach has been performed in order to determine sorption isotherm. Thus, 0.05 g of micro-HAP/nano-HAP was added to 50 mL of sample solutions containing various concentrations of Pb(II) and the *p*H was adjusted to 3.5. The contact time between the two phases was four hours to reach the equilibrium. After four hours, the filtrate solution was analyzed to assess the amount of Pb (II) ions remained in solution.

The experimental data obtained were fitted to both the Langmuir and Freundlich adsorption isotherms. According to Langmuir isotherm, the sorption of the adsorbate takes place as a monolayer adsorption onto a surface with a finite number of identical sites [39].

The equation 3 represents the equation characteristic to Langmuir model:

$$Q = \frac{K_L \cdot C_e}{1 + a \cdot C_e} \quad (3)$$

where:

Q - the maximum adsorption at monolayer (mg/g);

C_e - the equilibrium concentration of Pb(II) (mg/L);

K_L and a are the Langmuir model parameters.

Eq. 3 in linear form is expressed as:

$$\frac{C_e}{Q} = \frac{1}{K_L} + \left(\frac{a}{K_L}\right) \cdot C_e \quad (4)$$

The linear plots of Langmuir equation representing Pb(II) adsorption by micro-HAP and nano-HAP are illustrated in figure 13. These plots have been used to determine K_L and a parameters.

Another sorption model was proposed by Freundlich and it assumes that sorption takes place on heterogeneous surface being expressed in the form:

$$Q = K_F \cdot C_e^{1/n} \quad (5)$$

where K_F and n are Freundlich constants that show sorption capacity and intensity, respectively.

The logarithmic form of Freundlich equation is:

$$\log Q = \log K_F + n \log C_e \quad (6)$$

Freundlich parameters (K_F and n) have been determined from a linear plot of logQ against $\log C_e$ (fig. 14).

Table 1 contains the calculated adsorption constants of the Langmuir and Freundlich equations and their correlation coeffcients (R^2).

Based on the values of correlation regression coefficents (R^2) presented in table 1, it can be concluded that sorption of Pb(II) on both micro-HAP and nano-HAP is better defined by Langmuir model than Freundlich model. Thus, sorption of Pb(II) on both types of sorbents takes place as a monolayer adsorption onto specific sites.

The values of equilibrium capacities (Q_{max}) of lead ions on different sorbent based on hydroxyapatite from literature are presented comparatively in table 2.

Comparing the values of adsorption capacities of various hydroxyapatite sorbents reported in the literature with those obtained by this work, it can be concluded that both sorbents synthesised can effectively be used in attenuating of lead ions concentration in aqueous solutions.

Three kinetic models are commonly used in order to investigate the mechanism of sorption. These models are pseudo-first order equation of Lagergren based on solid capacity, pseudo-second order equation of Ho based on

Adsorbent/starting materials	Q_{max} (mg/g)	Reference
Carbonate hydroxyapatite (CHAP)/(eggshell waste)	94.3	[37]
Calcium hydroxyapatite/($CaCO_3$, H_3PO_4)	85	[40]
HAP samples/($Ca(OH)_2$, H_3PO_4)	79.56	[38]
Hydroxyapatite gel (Gel_25)/($CaCO_3$, H_3PO_4)	750	[41]
Hydroxyapatite powder (Powder_25)/($CaCO_3$, H_3PO_4)	750	[41]
Hydroxyapatite powder (Powder_105)/($CaCO_3$, H_3PO_4)	750	[41]
Ca-HA/($Ca(NO_3)_2$, $NH_4H_2PO_4$)	620	[42]
Commercial Ca-HA	104	[42]
Ca-HA/($Ca(NO_3)_2$, $(NH_4)_2HPO_4$)	470	[43]
Ca-HA/($Ca(NO_3)_2$, $(NH_4)_2HPO_4$)	144 - 426	[44]
Ca-HA/($CaCl_2$, H_3PO_4; $Ca(NO_3)_2$, $(NH_4)_2HPO_4$; $Ca(NO_3)_2$, K_2HPO_4)	330 – 450	[45]
Ca-HA/($Ca(NO_3)_2$, $(NH_4)_2HPO_4$)	430 - 700	[35]
Ca-HA containing 16 wt.% of carbonate/($Ca(CH_3COO)_2$, Na_2HPO_4, $NaHCO_3$)	1823	[46]
Hydroxyapatite/polyurethane composite foams/(Hypol 3000, Hap)	150	[47]
Hydroxyapatite/magnetite composite/($Ca(NO_3)_2$, KH_2PO_4, F_3O_4)	598.8	[48]
Natural apatite	82.88	[49]
HAP/($Ca(OH)_2$, H_3PO_4)	91.58	[49]
Hap/($Ca(OH)_2$, $NH_4H_2PO_4$)	46 ± 2	[50]
a-HAp/($Ca(OH)_2$, $NH_4H_2PO_4$, adipic acid)	50 ± 1	[50]
c-HAp/($Ca(OH)_2$, $NH_4H_2PO_4$, citric acid)	50 ± 1	[50]
2.5N-HAp/($Ca(OH)_2$, $NH_4H_2PO_4$, nitrilotris(methylene)triphosphonic acid)	47 ± 1	[50]
5N-HAp/($Ca(OH)_2$, $NH_4H_2PO_4$, nitrilotris(methylene)triphosphonic acid)	48 ± 1	[50]
Nanohydroxyapatite–alginate composite/(bovine bones, sodium alginate, calcium chloride)	236	[51]
micro-HAP/($CaHPO_4 \cdot 2H_2O$, $CaCO_3$)	88.46	This work
nano-HAP/($Ca(NO_3)_2 \cdot 4H_2O$, $(NH_4)_2HPO_4$)	102.45	This work

Table 2
ADSORPTION CAPACITIES OF Pb(II) IONS BY VARIOUS HYDROXYAPATITE SORBENTS

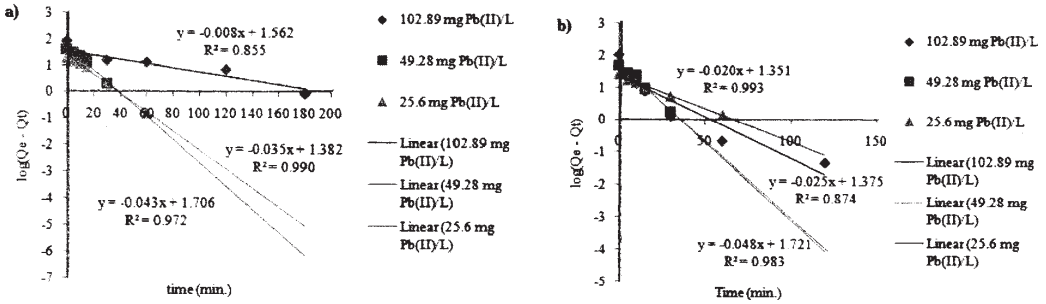

Fig. 15. Pseudo-first order sorption kinetics Pb(II) onto micro-HAP at 102.89 mg/L initial concentration, 49.28 mg/L initial concentration, and 25.6 mg/L initial concentration (a), and onto nano-HAP at 102.89 mg/L initial concentration, 49.28 mg/L initial concentration, and 25.6 mg/L initial concentration (b)

the solid phase sorption, and intraparticle diffusion equation [36].

According to the pseudo-first-order model, the rate of adsorption on sorbent is proportional to the number of active sites available onto sorbent media.

Lagergren equation that represents the mathematical expression of the pseudo-first-order model is the following [52]:

$$\frac{dQ_t}{dt} = k_1(Q_e - Q_t) \quad (7)$$

where: Q_e, Q_t are the sorption capacities at equilibrium and at time t (mg/g), and k_1 is the rate constant of pseudo-first order sorption (min^{-1}).

Equation (7) can be rearranged to obtain a linear form:

$$\log(Q_e - Q_t) = \log Q_e - \frac{k_1}{2.303} \cdot t \quad (8)$$

where Q_e and Q_t represent the amounts of Pb(II) retained on sorbent (mg/g) at equilibrium and at time t, respectively and k_1 is the first-order sorption rate constant (min^{-1}).

The slopes and intercepts of plot of $\log(Q_e - Q_t)$ versus t were used to obtain the first-order rate constant k_1 and the correlation coefficient R^2 (fig. 15).

Table 3 shows the values of k_1 and R^2 for the pseudo-first-order Lagergren model obtained from the plot of $\log(Q_e - Q_t)$ versus time.

The adsorption kinetic may also be described by the pseudo-second-order model using the Ho equation represented as:

$$\frac{t}{Q_t} = \frac{1}{k_2 Q_e^2} + \frac{t}{Q_e} \quad (9)$$

where k_2 is the rate constant of second-order adsorption (g/mg·min). Straight-line plots t/Q_t against t (fig. 16a and b) were used to determine kinetic parameters.

Sorbent	102.89 mg/L Pb(II)		49.28 mg/L Pb(II)		25.6 mg/L Pb(II)	
	k_1 (min^{-1})	R^2	k_1 (min^{-1})	R^2	k_1 (min^{-1})	R^2
micro-HAP	$1.8424 \cdot 10^{-2}$	0.855	$9.9029 \cdot 10^{-2}$	0.972	$8.0605 \cdot 10^{-2}$	0.990
nano-HAP	$5.7575 \cdot 10^{-2}$	0.874	$11.0544 \cdot 10^{-2}$	0.983	$4.606 \cdot 10^{-2}$	0.993

Table 3
THE RATE CONSTANT K_1 AND R^2 CORRELATION COEFFICIENT VALUES FOR PSEUDO-FIRST-ORDER EQUATION

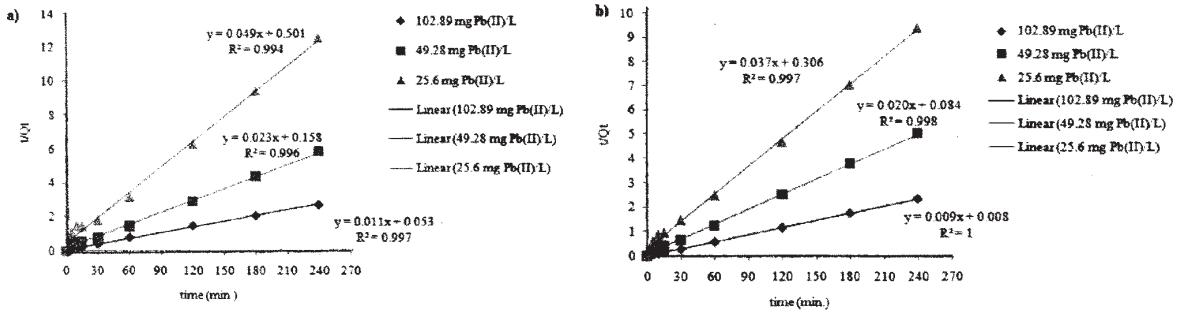

Fig. 16. Pseudo-second order sorption kinetics of Pb(II) onto micro-HAP at 102.89 mg/L initial concentration, 49.28 mg/L initial concentration, and 25.6 mg/L initial concentration (a), and nano-HAP at 102.89 mg/L initial concentration, 49.28 mg/L initial concentration, and 25.6 mg/L initial concentration (b)

Sorbent	102.89 mg/L Pb(II)		49.28 mg/L Pb(II)		25.6 mg/L Pb(II)	
	k_2 (g/mg·min)	R^2	k_2 (g/mg·min)	R^2	k_2 (g/mg·min)	R^2
micro-HAP	$2.2830 \cdot 10^{-3}$	0.997	$3.3481 \cdot 10^{-3}$	0.996	$4.7924 \cdot 10^{-3}$	0.994
nano-HAP	$1.0125 \cdot 10^{-2}$	1	$4.7619 \cdot 10^{-3}$	0.998	$4.4739 \cdot 10^{-3}$	0.997

Table 4
THE RATE CONSTANT K_2 AND R^2 CORRELATION COEFFICIENT VALUES FOR PSEUDO-SECOND ORDER EQUATION

The estimated reaction rate and the correlation coefficient (R^2) values of fitting the second-order rate model are comparatively reported in table 4 for both sorbents at different Pb(II) concentrations in the initial solution.

Based on the linear regression coefficients values (R^2>0.994) it can be concluded that the kinetic of lead sorption onto micro-HAP and nano-HAP can be described well by the second-order equation.

Weber and Morris [86] explored the possibility of intra-particle diffusion resistance to affect the sorption process. The intraparticle diffusion model may be expressed in the form:

$$Qt = k_i t^{0.5} \quad (10)$$

Where, k_i is the intra-particle diffusion rate constant (mg/g·min$^{0.5}$). The value of k_i is the slope obtained from the graphical representation of Q_t versus $t^{0.5}$ (fig. 17a and b).

From figures 17 a and b, it can be seen that there are two separate regions. The first region can be attributed to the film diffusion, and the second region is due to intraparticle diffusion. This trend was also observed by other researchers [53, 54]. Consequently, two values of k_i (k_{i1} and k_{i2}) were determined from the slopes of the two straight lines (figs. 18a, a' and 18b, b').

The kinetic parameters for intraparticle diffusion for lead sorption onto micro-HAP and nano-HAP are listed in table 5.

Experimental data on the kinetic of lead sorption by micro-and nano-HAP indicate that this process can be described in terms of pseudo-second order equation (R^2> 0.994). Thus, the rate-limiting step in lead sorption processes may be chemisorption involving covalent forces through the sharing or exchange electrons between HAP particles and lead ions. This was also reported by Ho and McKay [55].

The mechanism of lead removal by HAP

Different mechanisms have been developed for the retaining of Pb(II) on hydroxyapatite materials. The first mechanism assumes that sorption of lead ions takes place

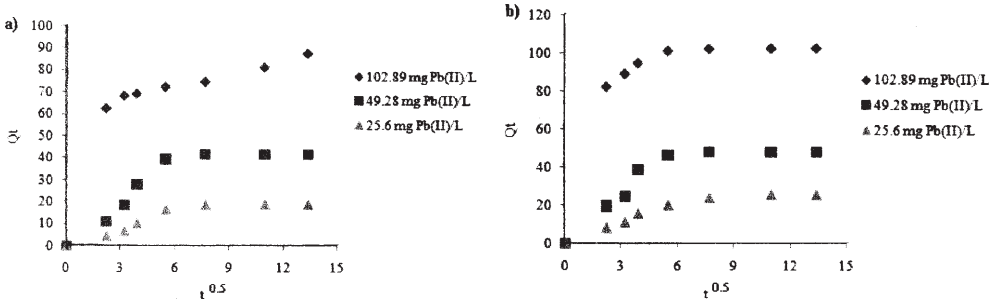

Fig. 17. Intraparticle diffusion sorption kinetics Pb(II) onto micro-HAP at 102.89 mg/L initial concentration, 49.28 mg/L initial concentration, and 25.6 mg/L initial concentration (a) and nano-HAP at 102.89 mg/L initial concentration, 49.28 mg/L initial concentration, and 25.6 mg/L initial concentration (b)

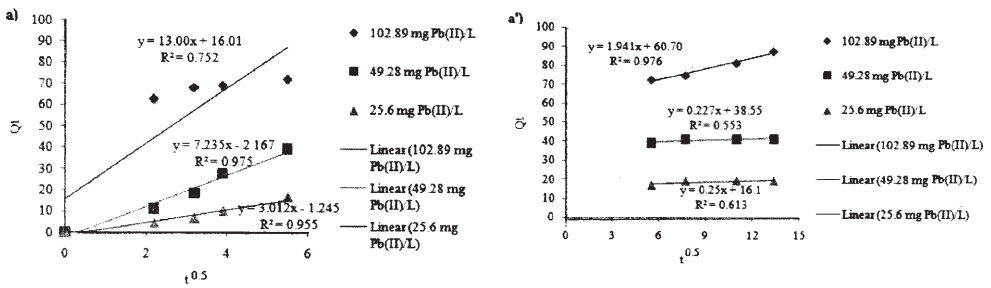

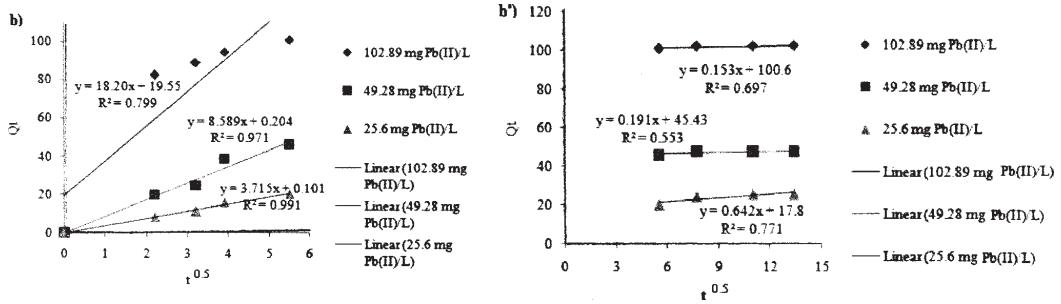

Fig. 18. Intraparticle diffusion sorption kinetics of Pb(II) onto micro-HAP at 102.89 mg/L initial concentration, 49.28 mg/L initial concentration, and 25.6 mg/L initial concentration separated in two regions (a, a'), and nano-HAP at 102.89 mg/L initial concentration, 49.28 mg/L initial concentration, and 25.6 mg/L initial concentration separated in two regions (b, b')

Pb(II) concentration (mg/L)	Sorbent			
	micro-HAP		nano-HAP	
102.89	k_{i1} (mg/mg·min$^{0.5}$)	R^2	k_{i1} (mg/mg·min$^{0.5}$)	R^2
	13	0.752	18.2	0.799
	k_{i2} (mg/mg·min$^{0.5}$)	R^2	k_{i2} (mg/mg·min$^{0.5}$)	R^2
	1.941	0.976	$1.53 \cdot 10^{-1}$	0.697
49.28	k_{i1} (mg/mg·min$^{0.5}$)	R^2	k_{i1} (mg/mg·min$^{0.5}$)	R^2
	7.235	0.975	8.589	0.971
	k_{i2} (mg/mg·min$^{0.5}$)	R^2	k_{i2} (mg/mg·min$^{0.5}$)	R^2
	$2.27 \cdot 10^{-1}$	0.553	$1.91 \cdot 10^{-1}$	0.553
25.6	k_{i1} (mg/mg·min$^{0.5}$)	R^2	k_{i1} (mg/mg·min$^{0.5}$)	R^2
	3.012	0.955	3.715	0.991
	k_{i2} (mg/mg·min$^{0.5}$)	R^2	k_{i2} (mg/mg·min$^{0.5}$)	R^2
	$2.5 \cdot 10^{-1}$	0.613	$6.42 \cdot 10^{-1}$	0.771

Table 5
THE RATE CONSTANTS K_{i1}, K_{i2} AND R^2 CORRELATION COEFFICIENT VALUES FOR INTRAPARTICLE DIFFUSION EQUATION

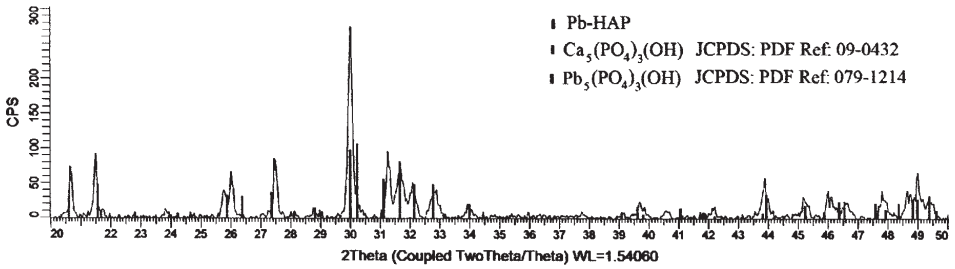

Fig. 19. X-ray pattern of micro-HAP loaded with Pb(II)

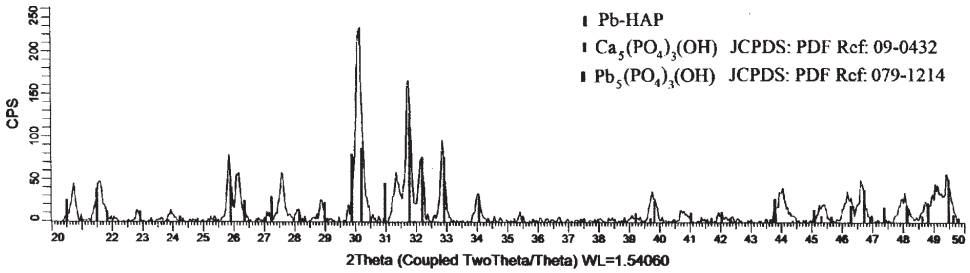

Fig. 20. X-ray pattern of nano-HAP loaded with Pb(II)

by dissolution of HAP followed by precipitation of lead hydroxyapatite or co-precipitation of lead-doped HAP [56]. The ionic exchange between calcium and lead ions is involved in the second mechanism [56].

In order to determine the mechanism involved in lead sorption by HAP, XRD measurements were performed onto micro- and nano-HAP loaded with lead ions. X-ray diffractograms are presented in figures 19 and 20.

X-ray diffraction patterns of both sorbents after sorption of Pb(II) (figs. 19 and 20) show distinct bands corresponding to the hydroxyapatite and hydroxy-pyromorphite phases ($Pb_5(PO_4)_3OH$). Therefore, in our case, the precipitation of Pb(II) is supported by the formation of hydroxy-pyromorphite ($Pb_5(PO_4)_3OH$). Furthermore, the fact that both diffractograms show peaks corresponding to the hydroxyapatite phase can lead to the conclusion that a dissolution – precipitation mechanism could occur partly at the surface of HAP particles. This mechanism is in agreement with the experimental results obtained from kinetic studies.

Effect of solution temperature

Temperature is considered an important factor influencing the process of sorption of pollutants from aqueous solutions.

In aquatic ecosystems, temperature changes depending on climate and therefore can be considered that natural water temperature varies within a certain range depending on the geographical area. However, numerous experiments were carried out in the laboratory at 25°C. This value does not always correspond to the temperature of natural water where effluents are discharged. Further studies regarding

Table 6
INFLUENCE OF TEMPERATURE ON THE LEAD SORPTION ON MICRO- AND NANO-HAP (INITIAL CONCENTRATION: 102.89 mg /L Pb(II))

Temperature (°C)	Residual Pb(II) concentration (mg/L)	Pb(II) amount retained/g micro-HAP (mg/g)	Temperature (°C)	Residual Pb(II) concentration (mg/L)	Pb(II) amount retained/g nano-HAP (mg/g)
21±2	0.44	88.46	21±2	14.43	102.45
30	34.26	61.33	30	41.56	68.63
40	40.93	51.91	40	50.98	61.96

the influence of the temperature on the sorption process can help to characterize the sorption process and to choose the optimal conditions for this [57].

Thus, a study about the effect of temperature on the sorption process of Pb(II) from aqueous solutions by micro- and nano-HAP particles was performed. The obtained data are given in table 6.

The data presented in table 6 show a decrease of Pb(II) amount retained both on micro- and nano-HAP with increasing of the temperature. Therefore, in terms of temperature the removal of Pb (II) from synthetic solutions using micro- and nano-HAP is performed with maximum efficiency at room temperature.

Conclusions

In this study, we used two simple methods (wet and dry chemical methods) for the synthesis of hydroxyapatite particles of nano and micrometric size. It has been evidenced that physical and chemical properties of hydroxyapatite, closely related to chemical reactivity, are strongly influenced by the preparation method and experimental conditions. All HAP samples were characterized by IR spectroscopy, SEM analysis, XRD and nitrogen sorption measurements. The XRD patterns of both types of HAP particles indicated that both samples contain no impurities. SEM analysis revealed that the wet synthesis method lead to nanometric HAP particles and the solid-phase sintering method allowed the obtaining of micrometric HAP particles. BET surface areas suggested a higher sorption capacity of nano-HAP powder than that of micro–HAP powder. Both powders obtained were comparatively tested for the sorption of lead ions from aqueous solutions. The results suggested that both of them are effective in attenuating lead ion in aqueous solutions. The nano-HAP has a higher lead removal efficiency than micro-HAP. The highest amount of Pb(II) ions retained by nano-HAP (102.45 mg/g) is in accordance with the literature data. The contact time of approximately 60-240 min was required to reach the equilibrium. The adsorption isotherms could be well defined by Langmuir equation. The experimental data were fitted by the second-order kinetic model that suggests that chemical sorption is the rate-limiting step.

X-ray diffractograms of both sorbents (micro and nano-HAP) loaded with lead ions were used to propose a mechanism of lead ions removal, It was suggested that the main mechanism consists in dissolution of HAP followed by the precipitation of different phases with higher lead content. The removal process has been performed with maximum efficiency at room temperature.

The results of this study demonstrate that synthetic hydroxyapatite powders are very goods candidates for substantially removal of lead ions from contaminated water.

Acknowledgments: The research was financed by the Ministry of National Education – Executive Unit for Financing Higher Education, Research and Development and Innovation (MEN – UEFISCDI) in the PARTNERSHIP in the priority areas PNII program through project PARTNERSHIP 92/01.07.2014.

References

1.WU, Q., TAM, N. F.Y., LEUNG, J.Y.S., ZHOU, X., FU, J., YAO, B., HUANG, X., XI, L, Ecotox. Environ. Safe. **104,** 2014, p. 143.
2. MODROGAN, C., PINCOVSCHI, I., BUDEA, S., Rev. Chim. (Bucharest) **65**, no. 10, 2014, p. 1235.
3. MODROGAN, C., PINCOVSCHI, I., Rev. Chim. (Bucharest) **65**, no. 11, 2014, p. 1253.
4] SIMONESCU, C.M., FERDES, M., Polish Journal of Environmental Studies, **21**(6) 2012, p. 1831.
5 LEMAIRE, J., SVECOVA, L., LAGALLARDE, F., LAUCOURNET, R., THIVEL, P-X., Hydrometallurgy **143**, 2014, p. 1.
6 . SIMONESCU, C.M., DIMA, R., FERDES, M., MEGHEA, A., Rev. Chim. (Bucharest), **63**, no. 2, 2012, p. 224.
7 DJUKIC, A., JOVANOVIC, U., TUVIC, T., ANDRIC, V., NOVAKOVIC, J.G., IVANOVIC, N., MATOVIC ,L., Ceram. Int. **39**(6), 2013, p. 7173.
8 SANCEY, B., TRUNFIO, G., CHARLES, J., MINARY, J-F., GAVOILLE, S., BADOT, P-M., CRINI, G., J. Environ. Manag. **92**(3), 2011, p. 765.
9. MODIN, H., PERSSON, K.M., ANDERSSON, A., van PRAAGH, M, J. Hazard. Mat. **189**(3), 2011, p. 749-.
10 HUA, M., ZHANG, S., PAN, B., ZHANG, W., LV, L., ZHANG, Q., J. Hazard. Mat. **211-212**, 2012, p. 317.
11. ROJAS, R., Appl Clay Sci. **87**, 2014, p. 254.
12.SHAHEENA, S.M., EISSA, F.I., GHANEM, K.M., GAMAL EL-DIN, H.M., AL ANANY, F.S., J. Environ. Manag. **128**, 2013, p. 514.
13. HOKKANEN, S., REPO, E., SILLANPÄÄ, M., Chem. Eng. J. **223**, 2013, p. 40.
14. SALAM, M.A., AL-ZHRANI, G., KOSA, S.A., J. Ind. Eng. Chem. **20**(2), 2014, p. 572.
15. FIGUEIREDO, H., QUINTELAS, C., J. HAZARD. Mat. **274**, 2014, p. 287.
16. SANKARARAMAKRISHNAN, N., JAISWAL, M., VERMA, N., Chem. Eng. J. **235**, 2014, p. 1.
17. MOULAY, S., BENSACIA, N., GARIN, F., FECHETE, I., BOOS, A., C.R. Chimie **17**, 2014, p. 849.
18. GONZÁLEZ-GÓMEZ, R., ORTEGA, A., LAZO, L.M., BURILLO, G., Radiat. Phys. Chem., 102, 2014, p. 117.
19. IVANETS, A.I., KITIKOVA, N.V., SHASHKOVA, I.L., OLEKSIIENKO, O.V., LEVCHUK, I., SILLANPÄÄ, M., J. Environ. Chem. Eng. 2(2), 2014, p. 981.
20. GIL, A., ALBENIZ, S., KORILI, S.A., Chem. Eng. J. **251**, 2014, p. 43.
21.VISA, M., CHELARU, A-M., Appl. Surf. Sci. **303**, 2014, p. 14.
22. GAUTAM, R.K., MUDHOO, A., LOFRANO, G., CHATTOPADHYAYA, M.C., J Environ. Chem. Eng. 2(1), 2014, p. 239.
23. ZHANG, Y., CHEN, Y., WANG, C., WEI, Y., J. Hazard. Mat. **276**, 2014, p. 129.
24. GRECU, M., NOVAC, G., IONITA, D., UNGUREANU, C., Rev. Chim. (Bucharest) **62**, no. 3, 2011, p. 352.
25. GUNDUZ, O., GODE, C., AHMAD, Z., GÖKÇE, H., YETMEZ, M., KALKANDELEN, C., SAHIN, Y.M., OKTAR, F.N., J. Mech. Behav. Biomed. Mater. **35**, 2014, p. 70.

26. PAJCHEL, L., KOWALSKA, V., SMOLEN, D., KEDZIERSKA, A., PIETRZYKOWSKA, E., LOJKOWSKI, W., KOLODZIEJSKI, W., Mater. Res. Bull. **48**(11), 2013, p. 4818.
27. MELINESCU, A., TARDEI, C., SIMONESCU C.M., MARINESCU, V., MICLEA, A., Romanian Journal of Materials, **43**(2)**,** 2013, p. 223.
28. TARDEI, C., SPATARU, M., ALBU, F.M., STOLERIU, S., ANGHEL IONCEA, Romanian Journal of Materials, 43(1), 2013, p. 41.
29. HAO, L., YANG, H., ZHAO, N., DU, C., WANG, Y., Powder Technol. **253**, 2014, p. 172.
30. KAYGILI, O., DOROZHKIN, S.V., KESER, S., Mater. Sci. Eng.C **42**, 2014, p. 78.
31. OKADA, M., FUJII, S., NISHIMURA, T., NAKAMURA, Y., TAKEDA, S., FURUZONO, T., Appl. Surface Sci. **26**2(1), 2012, p. 39.
32.POINESCU, A.A., RADULESCU, C., VASILE, B.S., IONITA, I., Rev. Chim. (Buharest), **65**, no. 10, 2014, p. 1245.
33. GOPI, D., KARTHIKA, A., NITHIYA, S., KAVITHA, L., Mater. Chem. Phys. **144**(1-2), 2014, p. 75.
34. GOPI, D., INDIRA, J., KAVITHA, L., SEKAR, M., MUDALI, U.K., Spectrochim. Acta Part A: Mol. Biomol. Spectrosc. 93, 2012, p. 131.
35. MOBASHERPOUR, I., SALAHI, E., PAZOUKI, M., Arab. J. Chem. **5**(4), 2012, p. 439.
36. LANDI, E., TAMPIERI, A., CELOTTI, G., SPRIO, S., J. Eur. Ceram. Soc. **20**, 2000, p. 2377.
37. SIMONESCU, C.M., MARIN, I., TARDEI, C., DRAGNE, M., CAPATINA, C., Rev. Chim. (Bucharest) **65**, no. 7, 2014, p. 750.
38.SMICIKLAS, I., ONJIA, A., RAICEVIC S., JANACKOVIC, D., MITRIC, M., J. Hazard. Mater. **152**, 2008, p. 876.
39. LIAO, D., ZHENG, W., LI, X., YANG, Q., YUE, X., GUO, L., ZENG, G., J. Hazard. Mater. **177**, 2010, p. 126.
40 MINH, D.P., TRAN, N.D., NZIHOU, A., SHARROCK, P., Chem. Eng. J., **232**, 2013, p. 128.
41. SHASHKOVA, I.L., RAT'KO, A.I., KITIKOVA, N.V., Colloids Surf. A: Physicochem. Eng. Aspects **160**(3), 1999, 207.
42. MAVROPOULOS, E., ROSSI, A.M., COSTA, A.M., PEREZ, C.A., MOREIRA, J.C., SALDANHA, M., Environ. Sci. Technol. **36**, 2002, p. 1625.
43. SUGIYAMA, S., ICHII, T., MATSUMOTO, H., HAYASHI, H., Adv. Environ. Res. **6**(3), 2002, p. 285.
44. BAILLIEZ, S., NZIHOU, A., BERNACHE-ASSOLANT, D., CHAMPION, E., SHARROCK, P., J. Hazard. Mater. A**139**, 2007, p. 443.
45. MIYAKE, M., WATANABE, K., NAGAYAMA, Y., NAGASAWA, H., SUZUKI, T., J. Chem. Soc. Faraday Trans. **86**, 1990, p. 2303.
46. JANG, S.H., MIN, B.G., JEONG, Y.G., LYOO, W.S., LEE, S.C., J. Hazard. Mater. **152**, 2008, p. 1285.
47. DONG, L., ZHU, Z., QIU, Y., ZHAO, J., Chem. Eng. J. **165**, 2010, p. 827.
48. KALUDJEROVIC-RADOICIC, T., RAICEVIC, S., Chem. Eng. J. **160**, 2010, p. 503.
49. SAOIABI, S., ACHELHI, K., MASSE, S., SAOIABI, A., LAGHZIZIL, A., CORADI, T., Colloids and Surfaces A: Physicochem. Eng. Aspects **419**, 2013, p. 180.
50.GOOGERDCHIAN F., MOHEB, A., EMADI, R., Chem. Eng. J. **200 – 202**, 2012, p. 471.
51. NGAH, W.S.W., ENDUD C.S., MAYANAR R., React. Funct. Polym. **50**, 2002, p. 181.
52.WEBER, W.J., MORRIS, J.C., J. Sanity Eng, Div. Am. Soc. Civ. Eng. **89**, 1963, p. 53.
53. ALLEN, S.J., MCKAY, G., KHADER, K.Y.H., Environ. Pollut. **56**, 1989, p. 39
54. ELKADY, M.F., MAHMOUD, M.M., ABD-EL-RAHMAN, H.M., J. Non-Cryst. Solids 357, 2011, p. 1118.
55. HO, Y.S., McKAY, G., Process Biochem. **34,** 1999, p. 451.
56. XU, H.Y., YANG, L., WANG, P., LIU, Y., PENG, M.S., J. Environ. Manage. **86**, 2008, p. 319.
57. WANG, L., YANG, Z., NIU, J., Chemosphere **82**, 2011, p. 895

Manuscript reveived: 5.02.2014